

A speckle noise suppression method in phase-only holographic display based on an improved Gerchberg–Saxton algorithm

Minjie Hua^{a,b}, Yun Chen^{a,b}, Tianshun Zhang^{a,b}, Mingxin Zhou^{a,b},
Wenlong Zou^{a,b,*}, Jianhong Wu^{a,b,*}

^a School of Optoelectronic Science and Engineering & Collaborative Innovation Center of Suzhou Nano Science and Technology, Soochow University, Suzhou 215006, China

^b Key Lab of Advanced Optical Manufacturing Technologies of Jiangsu Province & Key Lab of Modern Optical Technologies of Education Ministry of China, Soochow University, Suzhou 215006, China

ARTICLE INFO

Keywords:

Holographic display
Speckle noise suppression
Computer generated hologram
Signal domain
Defocus without fragmentation and fracture phenomenon

ABSTRACT

In this paper, a speckle noise suppression method in phase-only holographic display based on an improved Gerchberg–Saxton(GS) algorithm is proposed. The computer generated hologram(CGH) is calculated by employing triple-constraint Gerchberg–Saxton(TCGS) algorithm. The amplitude distribution and the phase distribution in the signal domain are simultaneously constrained as the desired distribution to suppress speckle noise, meanwhile, the phase distribution in the non-signal domain is also constrained to increase the uniformity of the reconstructed object. In addition, the setting of signal domain ratio has a great influence on the quality of the final reconstructed object. It is found that when the signal domain ratio accounts for 25%– 65%, the quality of the reconstruction is much better. Furthermore, by putting forward some restrictions on sample intervals, the multi-plane three-dimensional(3D) object calculated by TCGS algorithm will defocus without fragmentation and fracture phenomenon. Both simulation and experiment results show that the speckle contrast is lower than 0.05, which verifies the effectiveness of the algorithm.

1. Introduction

Holographic display technique is regarded as the most ideal technique to realize true three-dimensional(3D) display in the future. It has a wide range of application prospects in many fields because it can reconstruct 3D objects with full depth cues and solve the vergence-accommodation conflict(VAC) [1–4]. Especially with the development of computer technology and silicon-based chips in recent years, holographic display technique based on spatial light modulator(SLM) has attracted much interest of many scholars at home and abroad. However, the current SLMs are capable to display either the amplitude or the phase component of the complex amplitude hologram. Besides, the reconstructed object based on phase-only SLM has the advantages of high diffraction efficiency and no twin image, therefore it is more widely used in holographic display [5]. Nonetheless, holographic display based on phase-only display also suffers some serious problems, one of those is speckle noise [6,7].

The high coherence of laser light source is one of the most important physical causes of speckle noise. There have been numerous researches to suppress speckle noise. Until now, methods of speckle-noise suppression in holographic display based on phase-only SLM can be mainly divided into the following two kinds. One method is proposed to suppress speckle noise by reducing the temporal

* Correspondence to: Soochow University, 1st Shizi Street, Suzhou, China.

E-mail addresses: zouwenlong@suda.edu.cn (W. Zou), jhwu@suda.edu.cn (J. Wu).

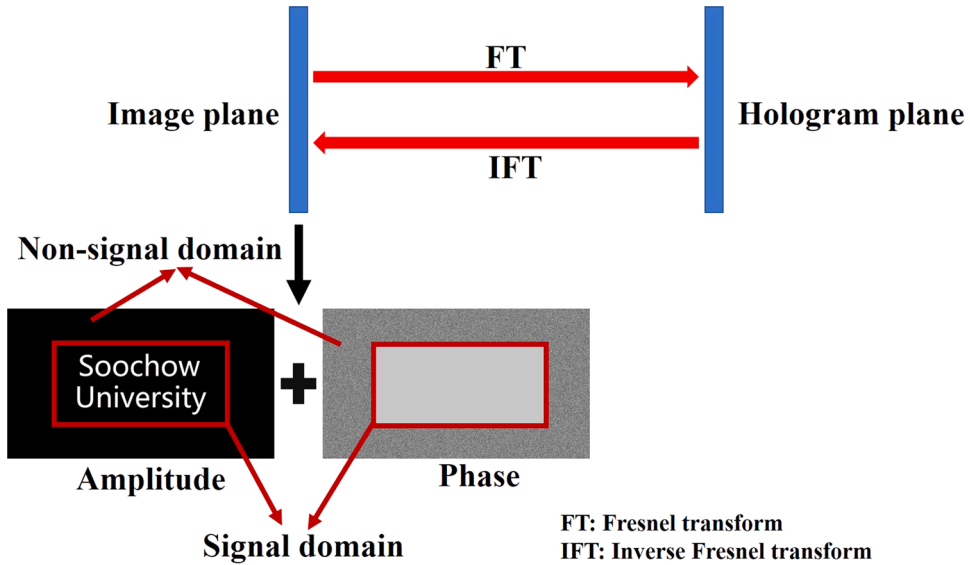


Fig. 1. Schematic diagram of TCGS algorithm.

coherence of light source, such as replacing the laser with LED [8,9], however, it is difficult to achieve the reconstructed objects with high sharpness and large depth of field. The other method is proposed to suppress speckle noise by reducing the spatial coherence of light source, such as introducing some diffractive optical elements [10–12], employing time multiplexing [13–16], pixel separation method [17–19] and optimizing both amplitude and phase distribution of the reconstructed object [20–25]. The first three methods are difficult to apply to dynamic display, while the last method does not have the disadvantage.

Generally, Gerchberg–Saxton(GS) algorithm is widely used to calculate phase-only CGH due to its fast-iterative convergence speed and accurate phase recovery [26–28]. It will introduce random phase before calculation to increase the scattering angle of target object. Hence, interference phenomenon will occur between adjacent pixels in the final holographic reconstruction due to the high coherence of laser and the random and uncontrollable phase distribution of each pixel on the reconstructed plane. This kind of extra chaotic interference intensity is usually called speckle noise. To suppress speckle noise, the most intuitive method is to simultaneously constrain amplitude and phase distribution as the desired distribution on the reconstructed plane during each iteration, thereby suppressing the occurrence of interference intensity. However, there is no free variable in the overall iterative optimization when amplitude and phase distribution are both set as constraints. Therefore, S.H. Tao et al. proposed a complex amplitude constraint algorithm. Before calculating the CGH, the target object is first divided into the signal domain(the domain with the effective information) and non-signal domain(the domain with invalid information). However, when Fourier or Fresnel diffraction transform formula is employed to calculate CGH based on complex amplitude constraint algorithm, the reconstructed objects will have the problem of uneven brightness [20]. To solve the problem, C.L. Chang et al. introduced three parameters to adjust the contrast and brightness of reconstructed objects, which is called double-constraint GS(DCGS) algorithm. The unevenness of reconstructed has a certain improvement, but it still exists. Precisely adjusting the three parameters in DCGS algorithm can overcome the problem of uneven brightness in the reconstructed objects based on complex amplitude constraint algorithm, but these three parameters have a large degree of freedom and it is difficult to find a set of relatively perfect parameters in a short time when changing the target objects. Furthermore, the DCGS algorithm is easy to fall into local convergence during the iteration, resulting in the unevenness of the reconstruction. Meanwhile, when DCGS algorithm is applied to calculate the CGH of multi-plane 3D object, the reconstructed object will defocus with fragmentation [21].

In order to solve these problems, this paper proposed an improved algorithm by employing triple-constraint GS(TCGS) algorithm, which increased one more constraint condition than complex amplitude constraint algorithm. The condition is added to improve the uniformity of reconstructed objects. Through this algorithm, we can quickly search for a better reconstructed result and speed up the calculation efficiency. Also, this paper specially analyzed the influence of signal domain ratio setting on the quality of reconstruction. In addition, when applying complex amplitude constraint algorithm into multi-plane 3D objects with improper sampling intervals which exceed the modulation capabilities of spatial light modulators, the phenomenon of defocusing with fragmentation and fracture will occur [21], this paper gave some derivations on sampling intervals. Meanwhile, the second and the third section gave the simulation and optical experiment results of TCGS algorithm respectively, and we drew the conclusion in the last Section.

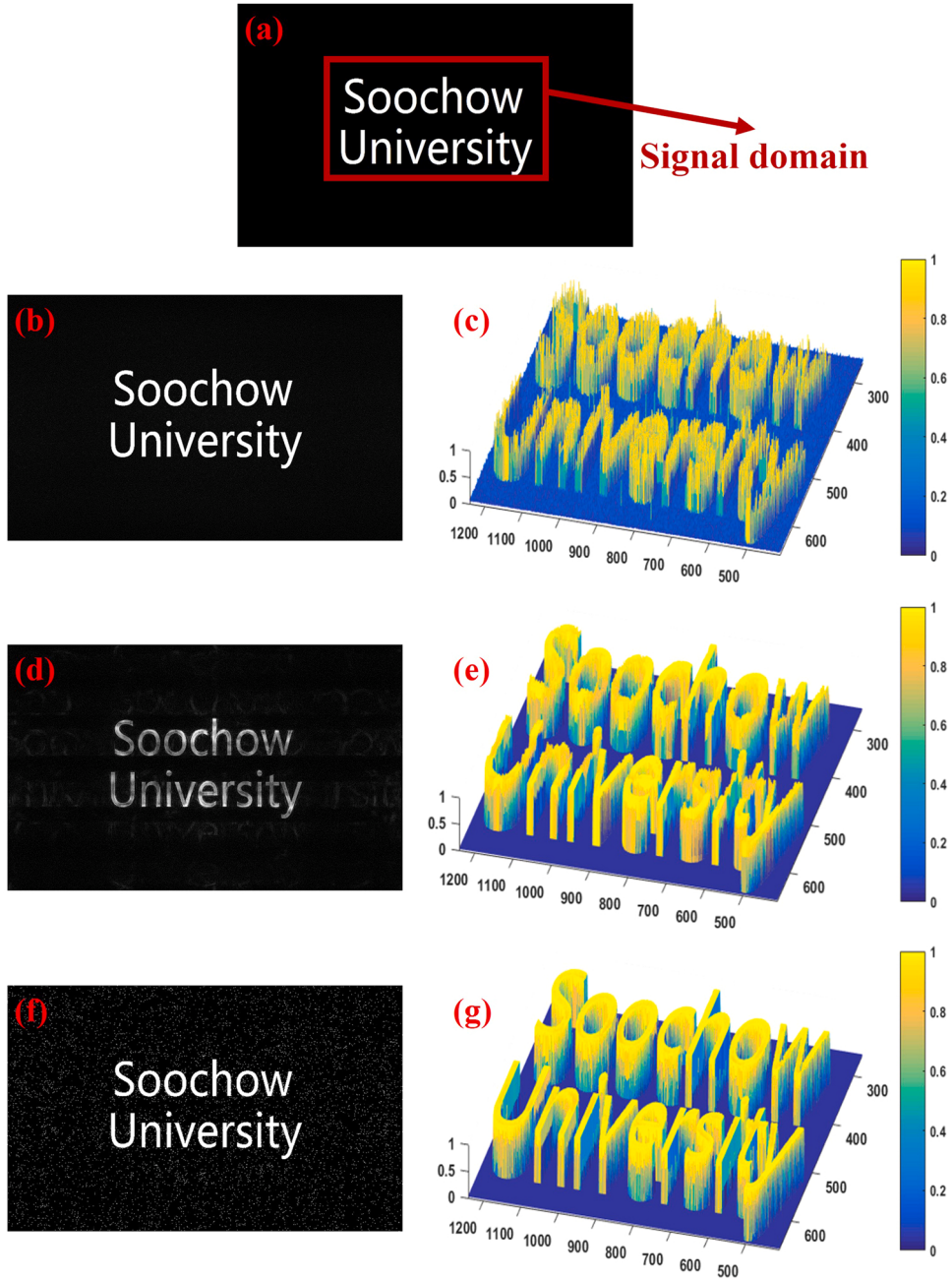


Fig. 2. Schematic diagram of comparison of three algorithms on the reconstructed plane. (a) Test image of 'Soochow University' letters. (b), (d), (f) Normalized amplitude distribution of reconstructed images from GS-based, DCGS-based and TCGS-based CGHs, respectively. (c), (e), (g) Normalized light intensity distribution of reconstructed images in the signal domain from GS-based, DCGS-based and TCGS-based CGHs, respectively.

2. Proposed method

2.1. The principle of TCGS algorithm

To solve these problems mentioned above, this paper proposed TCGS algorithm based on DCGS algorithm. DCGS algorithm ignored the phase distribution in the non-signal domain. For this reason, the phase distribution in the non-signal domain on the reconstructed plane is constrained to the fixed random distribution in each iteration, to make the algorithm jump out of local convergence, so that we can fast search for a better reconstructed result and speed up the calculation efficiency. The diagram of our proposed method is shown in Fig. 1. The complex amplitude distribution of the original object can be represented as:

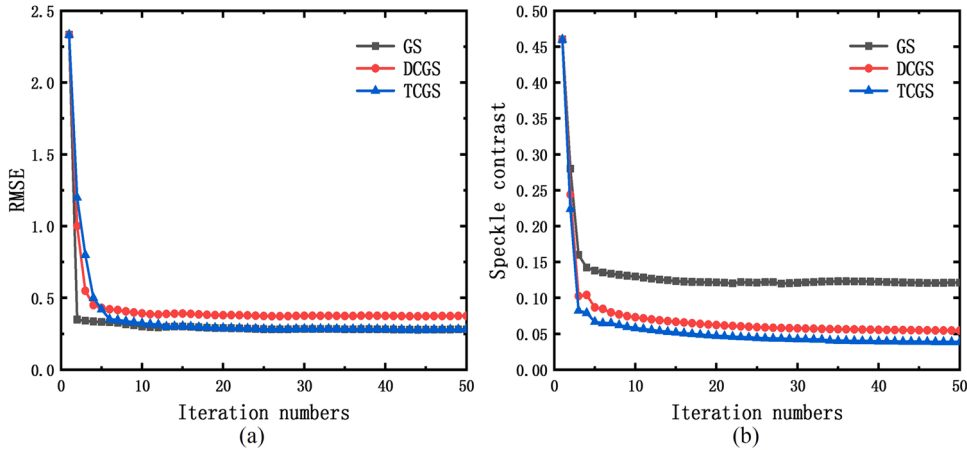


Fig. 3. Schematic diagram of comparison of the convergence among GS, DCGS and TCGS algorithm. (a) Results for RMSE. (b) Results for speckle contrast.

$$U_O(x, y) = A_O(x, y)\exp[i\varphi_{rO}(x, y)] \quad (1)$$

where x and y are the coordinate on the object plane. $A_O(x, y)$ and $\varphi_{rO}(x, y)$ represent the desired amplitude distribution and the original random phase distribution respectively. Here the transmission transformation formula between the image plane and the hologram plane is Fresnel diffraction formula, which is expressed as:

$$U_h(u, v) = \frac{1}{j\lambda z} \exp(jkz) \exp[j\frac{k}{2z}(u^2 + v^2)] \times \iint_{-\infty}^{\infty} U_O(x, y) \exp[j\frac{k}{2z}(x^2 + y^2)] \exp[-j\frac{2\pi}{\lambda z}(ux + vy) dx dy] \quad (2)$$

where u and v are the coordinate on the hologram plane. k and λ represent wave number and wavelength respectively. z represents the reconstructed distance between the image plane and the hologram plane. In each iteration, only the phase distribution is extracted and the amplitude distribution is replaced by the unity amplitude distribution on the hologram plane.

On the image plane, the amplitude distribution in the signal domain and the phase distribution in the signal and non-signal domain are all constrained in each iteration. The improved complex distribution on the reconstructed plane is expressed as follows:

$$G(x, y) = A_O(x, y) \bullet \exp[i\varphi_O(x, y)], \quad x, y \in SG(x, y) = \gamma \bullet A(x, y) \bullet \exp[i\varphi_{rO}(x, y)], \quad x, y \in N \quad (3)$$

in which S represents the signal domain, and N represents the non-signal domain. $A_O(x, y)$ and $A(x, y)$ represent the desired and the calculated amplitude distribution respectively, while $\varphi_O(x, y)$ and $\varphi_{rO}(x, y)$ represent the desired phase distribution in the signal and non-signal domain respectively on the reconstructed plane. Here $\varphi_O(x, y)$ is often set as uniform phase distribution and $\varphi_{rO}(x, y)$ is often set as the fixed random phase distribution. γ is used to adjust the brightness and contrast of reconstructions, the value of which is between 0 and 1. After several iterations, a hologram is generated, which can reconstruct objects with optimized complex amplitude distribution. Moreover, the interference phenomenon in the non-signal domain of the reconstructions based on TCGS algorithm is stronger than that of DCGS algorithm and increases the noise in the non-signal domain to a certain extent, but only the signal domain is effective in actual observation, so the problem can be ignored.

Next, we first tested reconstructions by computer simulation. The test image of size 1920×1080 is shown in Fig. 2(a). The signal domain is composed of 'Soochow University' letters. The CGHs are calculated after 20 iterations based on GS, DCGS and TCGS algorithm respectively, and the reconstructed distance is set to 800 mm. Here γ is set to 0.5. Fig. 2(b), Fig. 2(d) and Fig. 2(f) show the normalized amplitude distribution of reconstructed images from GS-based, DCGS-based and TCGS-based phase-only CGH, respectively. All three algorithms restored the amplitude distribution of the target image well, but it can be seen that the reconstructed image from DCGS-based CGH has obvious uneven brightness. While TCGS algorithm improves the uniformity of reconstructed image compared with DCGS algorithm due to constraining the phase distribution in the non-signal domain. Fig. 2(c), Fig. 2(e) and Fig. 2(g) show the normalized light intensity distribution of reconstructed images in the signal domain from GS-based, DCGS-based and TCGS-based phase-only CGH, respectively. Fig. 2(c) is very messy and has many fine peaks, resulting from speckle noise. As shown in Fig. 2(e) and Fig. 2(g), after constraining the phase distribution in the signal domain, the normalized light intensity distribution is very smooth, which proves the effectiveness of speckle-noise suppression.

Due to adding an extra constraint, it has some impacts on the convergence speed of the algorithm. In order to evaluate the convergence of the algorithm, this paper introduced root mean square error(RMSE) and speckle contrast(C) as the evaluation functions to test. The test image is shown in Fig. 2(a), which is composed of 'Soochow University' letters. The expressions of these two evaluation functions are shown in Eq.(4) and Eq.(5) [22,23]:

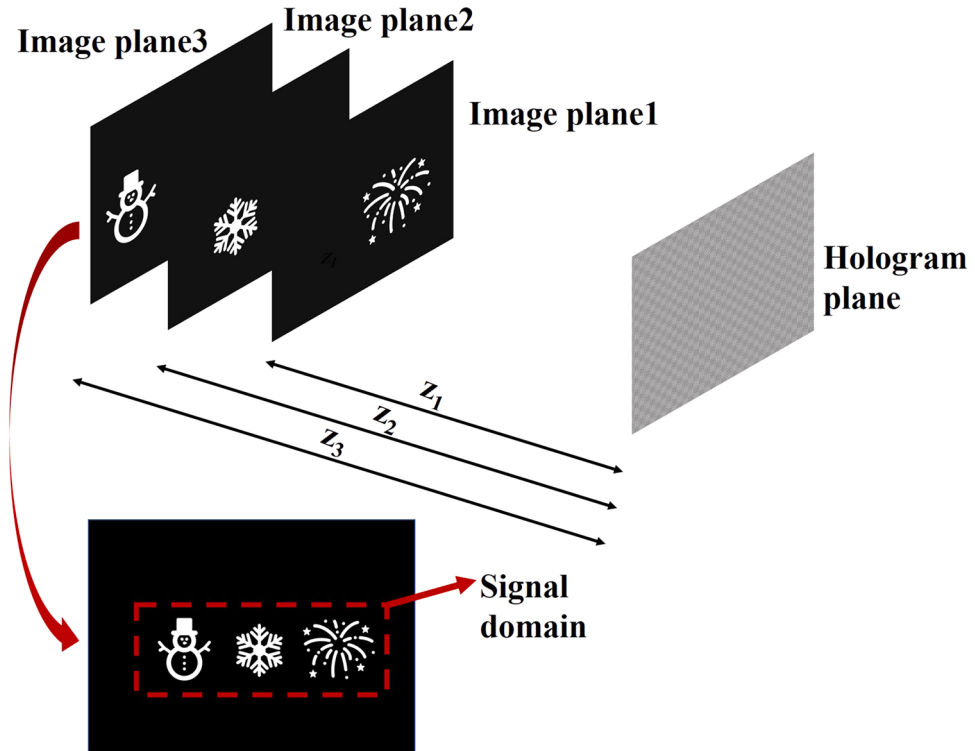


Fig. 4. Schematic diagram of TCGS algorithm for multi-plane 3D objects.

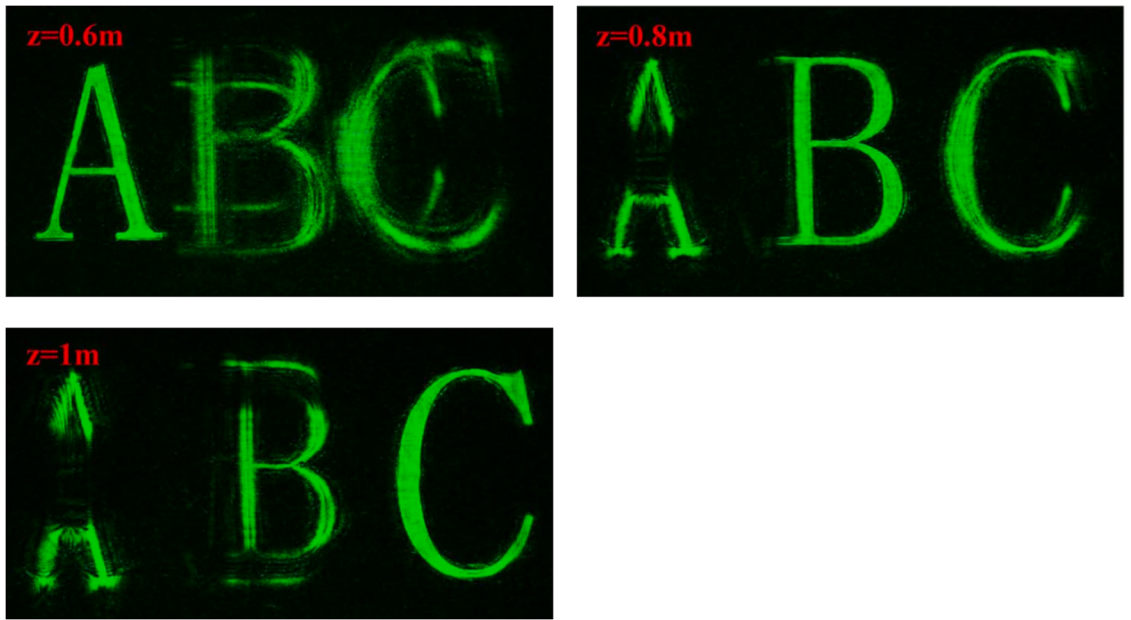


Fig. 5. Schematic diagram of multi-plane 3D object defocused with fragmentation and fracture phenomenon shown in Ref.21.

$$RMSE = \sqrt{\sum_{i=1}^M \sum_{j=1}^N (U'_{ij} - U_{ij})^2} \Bigg/ \sum_{i=1}^M \sum_{j=1}^N U_{ij}^2 \quad (4)$$

$$C = \sigma_I / \mu \quad (5)$$

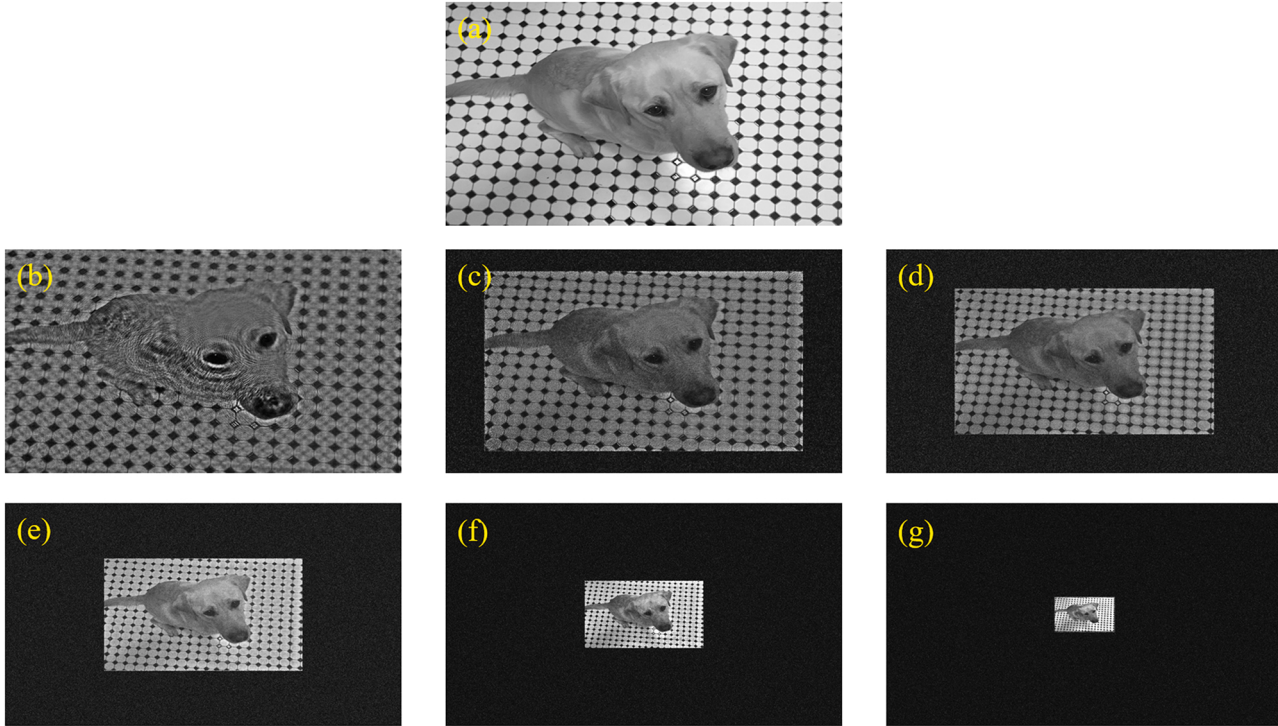


Fig. 6. Schematic diagram of comparison of influence of different signal domain ratios settings. (a) Test image ‘Kobi’. Reconstructions from different signal domain ratio setting. (b) 100%. (c) 80%. (d) 65%. (e) 50%. (f) 30%. (g) 15%.

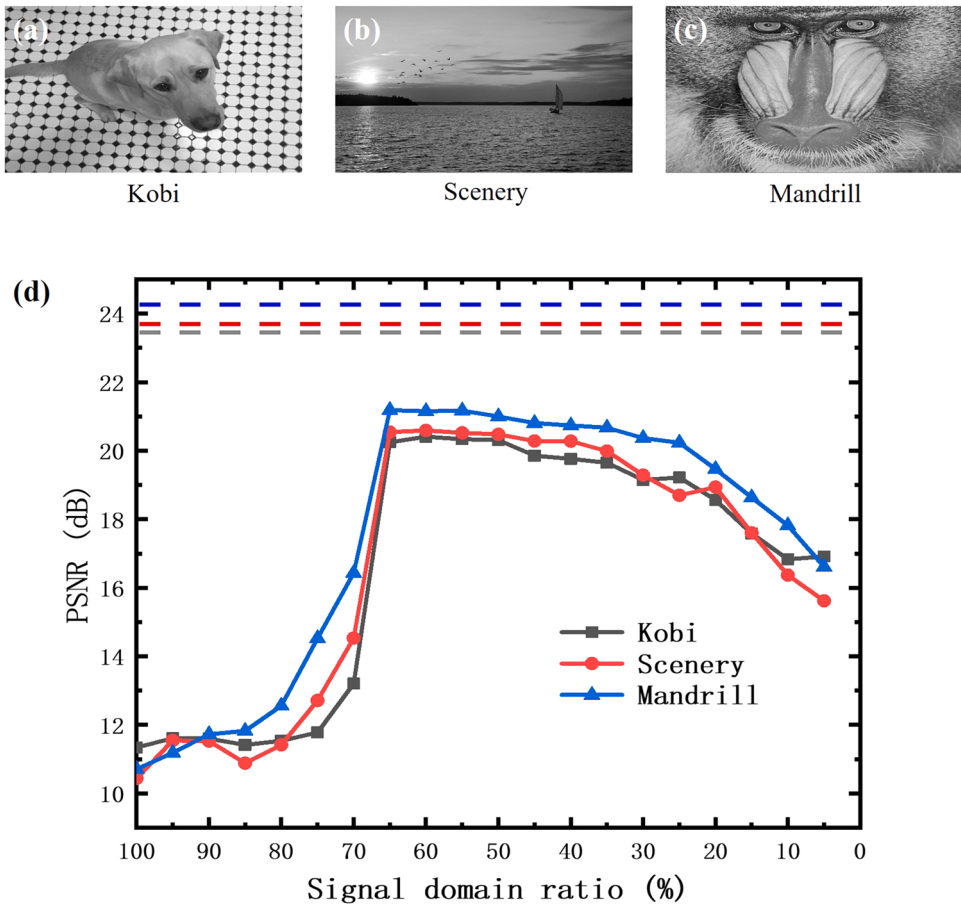


Fig. 7. Schematic diagram of PSNR with different signal domain ratios. (a) Test image ‘Kobi’. (b) Test image ‘Scenery’. (c) Test image ‘Mandrill’. (d) Graph.

in which M and N represent the pixel numbers in the horizontal and vertical direction of the test image. U_{ij} and U'_{ij} represent the desired and calculated amplitude distribution of the reconstructed object respectively. σ_I and μ represent the standard deviation and mean deviation of the normalized light intensity of the reconstructed object. It can be seen from Fig. 3(a) that with the increase of the constraints, the RMSE convergence speed of these three algorithms slows down in turn, but all these algorithms converge after 20 iterations. Due to the unevenness of reconstructed object, the RMSE convergence value of DCGS algorithm is much larger than other two algorithms. Also, from Fig. 3(b), we can see that the speckle noise of these algorithms tends to converge after 5 iterations. The speckle noise convergence value of GS algorithm is around 0.12, while the convergence value of DCGS and TCGS algorithm is around 0.05 and 0.03 respectively. Generally speaking, when the speckle contrast is lower than 0.05, it is considered that the algorithm can effectively suppress speckle noise. It can be obtained that TCGS and DCGS algorithm can effectively suppress speckle noise when the phase distribution of reconstructions is smooth.

2.2. TCGS algorithm for multi-plane 3D object

When further applying TCGS algorithm to calculate the CGH of multi-plane 3D object, it is similar to the expansion of GS algorithm [29,30]. First, the 3D object is sliced into several layers; then the signal domain of each layer is combined to acquire the total signal domain; finally, we use TCGS algorithm to calculate the CGHs of each layer and superimpose them to obtain the final CGH. Assuming that a multi-plane 3D object is composed of three separate planes as shown in Fig. 4, and the distances from the hologram plane are z_1 , z_2 and z_3 respectively. Each layer has its own signal domain, that is projected to the plane farthest from the hologram plane and taken the union to get the final signal domain. The final signal domain of the multi-plane 3D object is shown in the red dashed part. At each layer, we constrained both amplitude and phase distribution in the signal domain, meanwhile we constrained the phase distribution in the non-signal domain based on Eq.(3). Therefore, not only the speckle noise can be suppressed, but also the reconstructed objects can maintain uniformity.

As we know, TCGS algorithm is no random phase in the signal domain, when these algorithms without random phase are applied to calculating the CGH of multi-plane 3D objects, if the sampling intervals are set incorrectly or beyond the modulation capability of SLM,

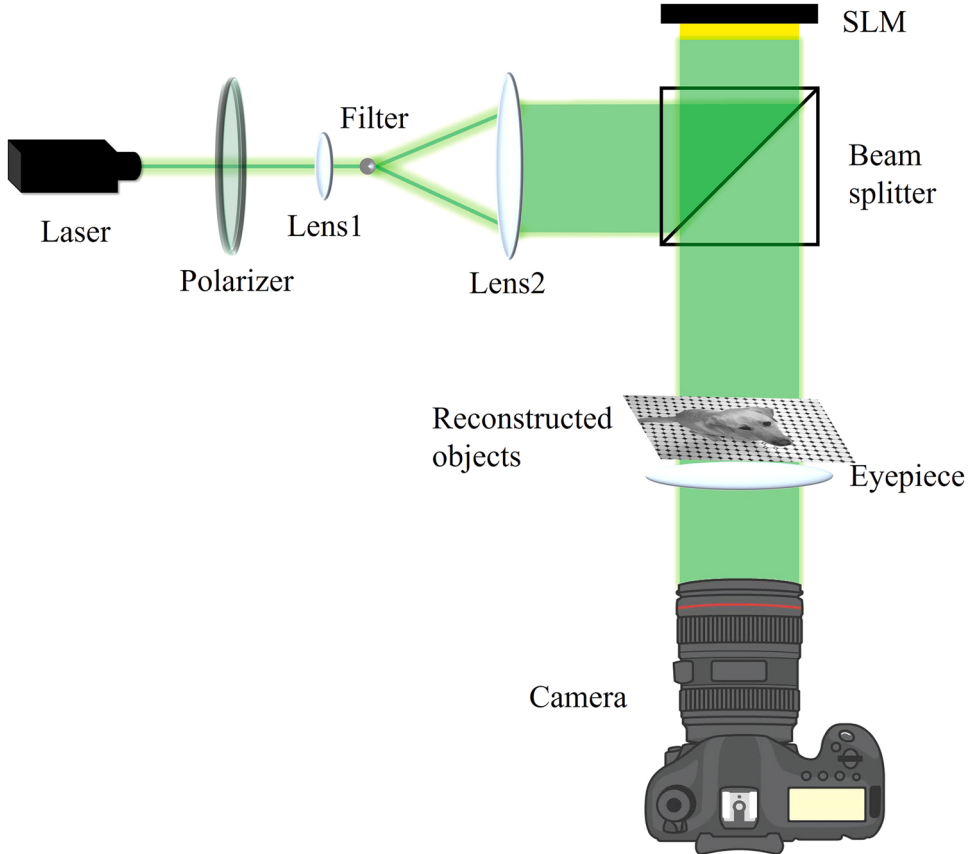


Fig. 8. Schematic diagram of optical setup for phase-only holographic display.

the reconstructed objects will defocus with fragmentation and fracture phenomenon, as shown in Fig. 5 [21]. This kind of defocusing phenomenon is obviously not in line with the normal phenomenon that the image becomes blurred when defocusing, which seriously affects the observation. To overcome the problem, we put forward some restrictions on sample intervals. The correct setting of sampling intervals will be expressed as follows.

Assuming that the sampling intervals of the object plane and hologram plane in the horizontal and vertical direction are Δx_o , Δy_o and Δu , Δv , respectively. According to the definition of local spatial frequency, the maximum of the spatial frequency on the object plane are expressed as:

$$\left\{ \begin{array}{l} f_{Oxmax} = \frac{M/2}{\lambda z} \Delta x_o \\ f_{Oymax} = \frac{N/2}{\lambda z} \Delta y_o \end{array} \right\} \quad (6)$$

in which M and N the pixel numbers in the horizontal and vertical direction. λ and z represent the wavelength and reconstructed distance. Therefore, according to Nyquist sampling theorem, the sampling intervals on the object plane needs to meet the following expression:

$$\left\{ \begin{array}{l} \frac{1}{2\Delta x_o} \geq f_{Oxmax} \\ \frac{1}{2\Delta y_o} \geq f_{Oymax} \end{array} \right. \Rightarrow \left\{ \begin{array}{l} \Delta x_o^2 \leq \frac{\lambda z}{M} \\ \Delta y_o^2 \leq \frac{\lambda z}{N} \end{array} \right\} \quad (7)$$

Considering the structural parameters and the modulation capability of the SLM, assuming that the pixel pitch of the SLM is p , the minimum sampling interval on the hologram plane is p . Generally, in order to ensure the image quality, the sampling interval on the hologram plane is set to p . Finally, the sampling intervals on the object plane and hologram plane are expressed as:

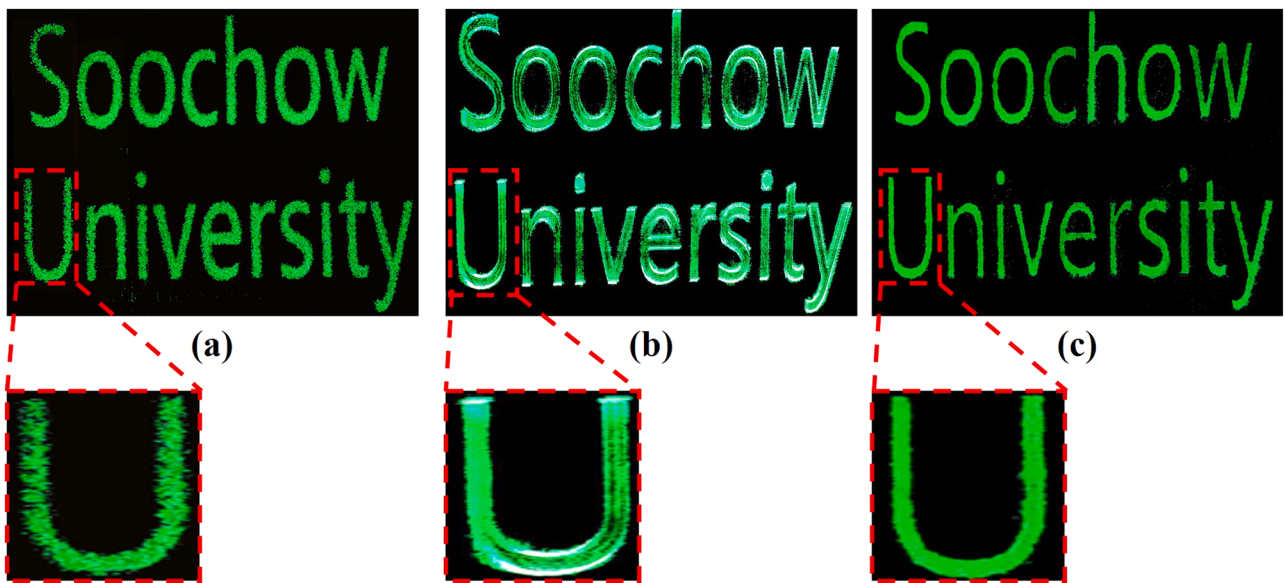


Fig. 9. Schematic diagram of reconstructed images from (a) GS-based CGH. (b) DCGS-based CGH. (c) TCGS-based CGH.

Table 1

Speckle contrast of three reconstruction results in Fig. 9.

	<i>GS algorithm</i>	<i>DCGS algorithm</i>	<i>TCGS algorithm</i>
<i>Speckle contrast</i>	0.243	0.058	0.036

$$\left\{ \begin{array}{l} \Delta x_o \leq \sqrt{\frac{\lambda z}{M}} , \quad \Delta y_o \leq \sqrt{\frac{\lambda z}{N}} \\ \Delta u = p , \quad \Delta v = p \end{array} \right\} \quad (8)$$

at this time, the reconstructed distance z needs to be satisfied $z \geq \max(\frac{f_o}{\lambda}, \frac{Mp^2}{\lambda}, \frac{Np^2}{\lambda})$. Hence, when all the planes of the multi-plane 3D object meet this sample interval requirements, there will be no defocusing with fragmentation and fracture phenomenon.

2.3. The setting of the signal domain ratio in TCGS algorithm

Before employing TCGS algorithm to calculate the CGH, the target image needs to be divided into signal domain and non-signal domain, but when the target image is a full-resolution image, it is necessary to artificially add a non-signal domain. This section is to explore the influence of the signal domain ratio setting on the quality of the reconstructed objects. Here we introduced the peak signal-to-noise ratio(*PSNR*) [22] to evaluate the amount of object information.

$$PSNR(U_o, U) = 10\log_{10}(255^2 / (\frac{1}{MN} \sum_{i=1}^M \sum_{j=1}^N (U_{oij} - U_{ij})^2)) \quad (9)$$

in which U_o and U represent the normalized amplitude distribution of target and calculated image respectively. M and N represent the pixel numbers in horizontal and vertical direction of the test image. From Eq.(9) we can see that the larger *PSNR* is, the larger the amount of information contained in objects is.

Next, we performed a simulation experiment on Kobi picture with a resolution of 1920×1080 as shown in Fig. 6(a), which is defined as the signal domain. The signal domain is scaled in the range of 1920×1080 , and we tested the influence of different settings of signal domain ratio(the ratio of the pixel numbers on the side of the signal domain to that of the entire image) on reconstruction quality. The reconstructed distance is set to 800 mm and γ is set to 0.5. Fig. 6(b)-(g) indicate the reconstructed images based on TCGS algorithm when the signal domain accounts for 100%, 80%, 65%, 50%, 30% and 15% respectively. It can be seen that the smaller the signal domain is, the more concentrated the energy is and the brighter the signal domain is. In order to ensure that the amount of object information remains unchanged, the nearest interpolation method is used to enlarge the reconstructed objects to the size of original object(1920×1080), and then calculate the *PSNR* of reconstructions. The *PSNR* of the six reconstructed images are calculated respectively, which are 11.339 dB, 11.535 dB, 20.246 dB, 20.340 dB, 19.148 dB, and 17.586 dB.

To verify that different ratios of the signal domain have a common effect on the amount of object information, the following three grayscale images of Kobi, Scenery and Mandrill shown in Fig. 7(a)-(c) are tested. The size of these images are all set to 1920×1080 , and the reconstructed distance is set to 800 mm and γ is set to 0.5. When the signal domain is different, the *PSNR* graph is shown in Fig. 7(d). *PSNR* is used as a measure of the amount of object information, which is affected by the reconstruction quality and the signal domain ratio. It can be seen from the change trend of the graph that when the signal domain ratio accounts for more than 80%, although the resolution of the signal domain is large, reconstruction quality is quite poor, resulting in a very low *PSNR*. When the signal domain ratio accounts for 65%– 80%, the *PSNR* increases as the signal domain ratio decreases and the reconstruction quality gradually increases. When the signal domain ratio accounts for 25%– 65%, the *PSNR* gradually stabilizes and the amount of object information becomes stable. When the signal domain ratio accounts for less than 25%, the *PSNR* drops because the loss of the object resolution is too much, and the amount of object information will be greatly lost. The dotted line in Fig. 7(d) is the *PSNR* of the reconstructions calculated by Burch coding, which is always considered to have lost half the amount of object information. The *PSNR* of the reconstructions from TCGS-based CGH is a little lower than that from Burch-based CGH, but the reconstructions based on phase coding has a much higher diffraction efficiency than that based on amplitude coding [5]. In actual experiments, under the premise of ensuring the reconstruction quality and amount of object information, the signal domain ratio is generally set to 25%– 65%.

3. Optical experiments and discussion

Figure 8 shows the optical setup for phase-only holographic display experiment. The 532 nm laser first passes through a polarizer, and then is collimated and expended by a spatial filter system, which is composed of lens1, a filter and lens2. Next, the expended beam is incident on the SLM through a beam splitter. The SLM used here is a Holoeye Pluto with resolution of 1920×1080 and pixel pitch of $8\mu m$. After being modulated by the SLM, the reconstructed object is obtained by Fresnel diffraction, which passes through the eyepiece and is captured by the camera. The camera used here is Cannon EOS 6D Mark II.

The following is an optical experiment on ‘Soochow University’ letters shown in Fig. 2(a). The signal domain ratio accounts for 45%, the reconstructed distance and γ are still set to 800 mm and 0.5. The reconstructions from GS-based, DCGS-based and TCGS-based CGH are shown in Fig. 9(a)-(c). Consistent with the simulation results, there is obvious speckle noise in the reconstructed

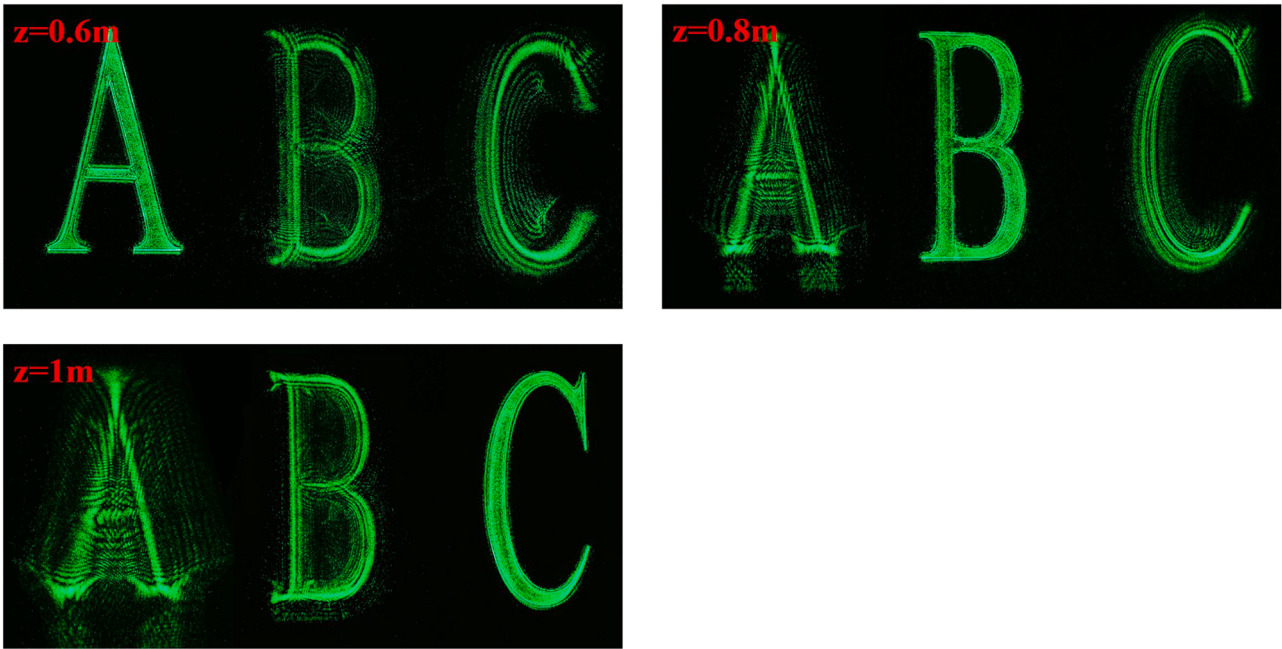


Fig. 10. Schematic diagram of multi-plane 3D object defocused without fragmentation and fracture phenomenon after changing sampling interval.

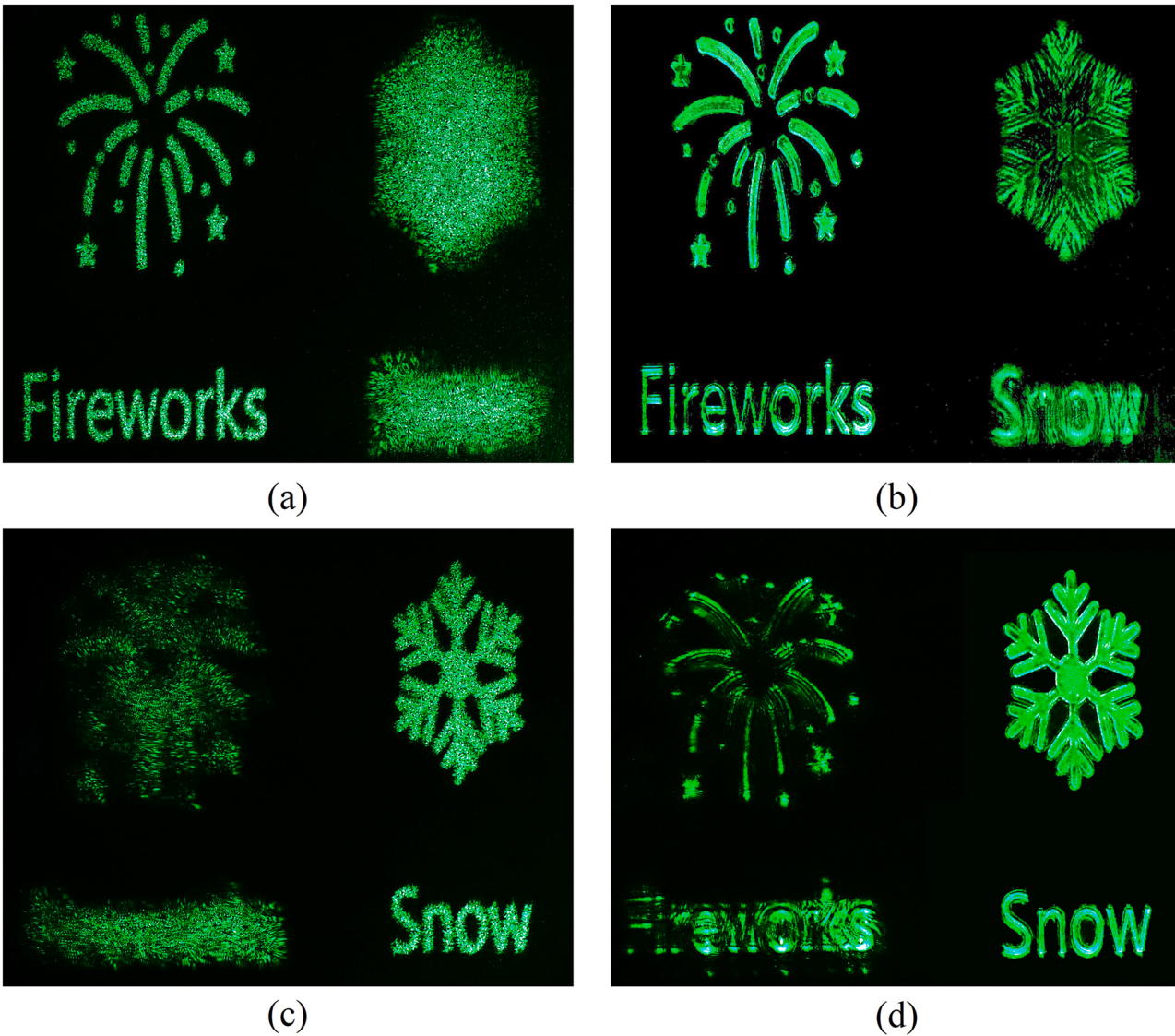


Fig. 11. Schematic diagram of comparison of multi-plane 3D objects from GS-based and TCGS-based CGH. (a) and (b) Focus on the 'Fireworks' plane. (c) and (d) Focus on the 'Snow' plane.

Table2

Speckle contrast of reconstruction results in Fig. 10.

	<i>GS algorithm</i>	<i>TCGS algorithm</i>
Focus on ‘Fireworks’ plane	0.231	0.048
Focus on ‘Snow’ plane	0.248	0.043

image from GS-based CGH, while the reconstructed images from DCGS-based and TCGS-based CGH are very smooth. It is because that the phase distributions in the signal domain based on these two algorithms are both strictly constrained, that greatly suppresses the speckle noise. However, comparing Fig. 9(b) and Fig. 9(c), it can be clearly seen that the reconstruction from TCGS-based CGH has uniform brightness, and the reconstructed quality is much better.

The three reconstruction results are further quantitatively analyzed, and the speckle contrast mentioned in Eq.(5) is calculated, as shown in Table1. The speckle contrast of the reconstruction from TCGS-based CGH is less than 0.05, proving this method can suppress the speckle noise again.

Next, we carried out the experiment on the multi-plane 3D object. To prove the effectiveness of changing the sampling interval to prevent 3D objects from defocusing with fragmentation and fracture phenomenon, we used Eq.(8) to calculate sampling interval when hologram calculation. Here we set $\Delta x_O = 12.8\mu m$, $\Delta y_O = 17.2\mu m$, $\Delta u = \Delta v = 8\mu m$. The reconstruction is shown in Fig. 10. Compared with Fig. 5, when setting the sampling interval correctly, the 3D objects will defocus without fragmentation and fracture phenomena, which is more in line with normal phenomena.

Furthermore, to prove our method can effectively suppress speckle noise of 3D objects, we tested the 3D object composed of two planes, one of that is ‘Fireworks’ and the other is ‘Snow’. The reconstructed distances from each plane to the hologram plane are 800 mm and 1000 mm. γ is set to 0.5. The total signal domain ratio of these two planes accounts for 45% and we utilized the method mentioned in Section 2.2 to calculate the CGH for 3D object. Here we compared the reconstructions with that from GS-based CGH. When camera focus on the plane that ‘Fireworks’ exists or the plane that ‘snow’ exists, the captured reconstruction results are shown in Fig. 11. It can be seen that the reconstruction results are both have a sense of depth. When focusing on the plane that ‘Fireworks’ exists, the ‘Fireworks’ image is clear, while the ‘Snow’ image becomes blur due to defocus. Moreover, the reconstruction from TCGS-based CGH on the focal plane is very smooth rather than grainy. The speckle contrast of the reconstructions is shown in Table2. The calculation results show that TCGS algorithm has a great effect on suppressing speckle noise of multi-plane 3D object.

4. Conclusions

In summary, this paper proposed a method to effectively suppress speckle noise in phase-only holographic display while ensuring the uniformity of the reconstructions by constraining the amplitude and phase distribution in the signal domain and the phase distribution in the non-signal domain. In each iteration, we constrained the phase distribution in the signal domain as uniform distribution, so as to reduce the interference between adjacent pixels and suppress the speckle noise. We further explored the influence of different signal domain ratio settings on the quality of reconstructions and gave the commonly used signal domain ratio setting. Moreover, this paper analyzed the sampling interval restrictions during the CGH calculation to prevent multi-plane 3D object from defocusing with fragmentation phenomenon. In the next work, we will explore a more appropriate form of phase distribution constraint and adjust the energy ratio of the signal domain and the non-signal domain to further improve the quality of the reconstructed objects. In short, this method has a great prospect in phase-only holographic display.

Declaration of Competing Interest

The authors declare that they have no known competing financial interests or personal relationships that could have appeared to influence the work reported in this paper.

Acknowledgements

This work was supported by Priority Academic Program Development (PAPD) of Jiangsu Higher Education Institutions, China and the Strategic Priority Research Program of Chinese Academy of Sciences, China (Grant No. XDA25020314).

References

- [1] F. Yaras, H. Kang, L. Onural, State of the art in holographic displays: a survey, *J. Disp. Technol.* 6 (2010) 443–454, <https://doi.org/10.1109/jdt.2010.2045734>.
- [2] Z.Q. Zhang, J. Liu, X.H. Duan, Y.T. Wang, Enlarging field of view by a two-step method in a near-eye 3D holographic display, *Opt. Express* 28 (2020) 32709–32720, <https://doi.org/10.1364/oe.403538>.
- [3] Y. Chen, M.J. Hua, T.S. Zhang, M.X. Zhou, J.H. Wu, W.L. Zou, Holographic near-eye display based on complex amplitude modulation with band-limited zone plates, *Opt. Express* 29 (2021) 22749–22760, <https://doi.org/10.1364/OE.431032>.
- [4] Y.F. Su, Z.J. Cai, L.Y. Shi, F. Zhou, P.L. Guo, Y.F. Lu, J.H. Wu, A multi-plane optical see-through holographic three-dimensional display for augmented reality applications, *Optik* 157 (2018) 190–196, <https://doi.org/10.1016/j.jleo.2017.11.081>.
- [5] T. Shimobaba, T. Kakue, Y. Endo, R. Hirayama, D. Hiyama, S. Hasegawa, Y. Nagahama, M. Sano, M. Oikawa, T. Sugie, T. Ito, Random phase-free kinoform for large objects, *Opt. Express* 23 (2015) 17269–17274, <https://doi.org/10.1364/oe.23.017269>.

- [6] Y.B. Deng, D.P. Chu, Coherence properties of different light sources and their effect on the image sharpness and speckle of holographic displays, *Sci. Rep.* 7 (2017) 12, <https://doi.org/10.1038/s41598-017-06215-x>.
- [7] N.N. Li, D. Wang, Y.L. Li, Q.H. Wang, Method of curved composite hologram generation with suppressed speckle noise, *Opt. Express* 28 (2020) 34378–34389, <https://doi.org/10.1364/oe.406265>.
- [8] F. Yaras, H.J. Kang, L. Onural, Real-time phase-only color holographic video display system using LED illumination, *Appl. Opt.* 48 (2009) H48–H53, <https://doi.org/10.1364/ao.48.000h48>.
- [9] M. Chlipala, T. Kozacki, Color LED DMD holographic display with high resolution across large depth, *Opt. Lett.* 44 (2019) 4255–4258, <https://doi.org/10.1364/ol.44.004255>.
- [10] D. Lee, C. Jang, K. Bang, S. Moon, G. Li, B. Lee, Speckle reduction for holographic display using optical path difference and random phase generator, *IEEE Trans. Ind. Inform.* 15 (2019) 6170–6178, <https://doi.org/10.1109/tii.2019.2927454>.
- [11] Y. Kuratomi, K. Sekiya, H. Satoh, T. Tomiyama, T. Kawakami, B. Katagiri, Y. Suzuki, T. Uchida, Speckle reduction mechanism in laser rear projection displays using a small moving diffuser, *J. Opt. Soc. Am. A-Opt. Image Sci. Vis.* 27 (2010) 1812–1817, <https://doi.org/10.1364/josaa.27.001812>.
- [12] W.F. Hsu, M.H. Weng, Compact holographic projection display using liquid-crystal-on-silicon spatial light modulator, *Materials* 9 (2016) 9, <https://doi.org/10.3390/ma9090768>.
- [13] W.F. Hsu, C.F. Yeh, Speckle suppression in holographic projection displays using temporal integration of speckle images from diffractive optical elements, *Appl. Opt.* 50 (2011) H50–H55, <https://doi.org/10.1364/ao.50.000h50>.
- [14] Y. Takaki, M. Yokouchi, Speckle-free and grayscale hologram reconstruction using time-multiplexing technique, *Opt. Express* 19 (2011) 7567–7579, <https://doi.org/10.1364/oe.19.007567>.
- [15] L. Golani, S. Shoham, Speckle elimination using shift-averaging in high-rate holographic projection, *Opt. Express* 17 (2009) 1330–1339, <https://doi.org/10.1364/oe.17.001330>.
- [16] L. Xin, D. Xiao, Q.H. Wang, Method to suppress speckle noise using time multiplexing in phase-only holographic display, *J. Soc. Inf. Disp.* 28 (2020) 641–647, <https://doi.org/10.1002/jsid.861>.
- [17] S.J. Liu, D. Wang, Q.H. Wang, Speckle noise suppression method in holographic display using time multiplexing technique, *Opt. Commun.* 436 (2019) 253–257, <https://doi.org/10.1016/j.optcom.2018.12.038>.
- [18] M. Makowski, Minimized speckle noise in lens-less holographic projection by pixel separation, *Opt. Express* 21 (2013) 29205–29216, <https://doi.org/10.1364/oe.21.029205>.
- [19] I. Ducin, T. Shimobaba, M. Makowski, K. Kakarenko, A. Kowalczyk, J. Suszek, M. Bieda, A. Kolodziejczyk, M. Sypek, Holographic projection of images with stepless zoom and noise suppression by pixel separation, *Opt. Commun.* 340 (2015) 131–135, <https://doi.org/10.1016/j.optcom.2014.11.100>.
- [20] S.H. Tao, W.X. Yu, Beam shaping of complex amplitude with separate constraints on the output beam, *Opt. Express* 23 (2015) 1052–1062, <https://doi.org/10.1364/oe.23.001052>.
- [21] C.L. Chang, J. Xia, L. Yang, W. Lei, Z.M. Yang, J.H. Chen, Speckle-suppressed phase-only holographic three-dimensional display based on double-constraint Gerchberg-Saxton algorithm, *Appl. Opt.* 54 (2015) 6994–7001, <https://doi.org/10.1364/ao.54.006994>.
- [22] Y.J. Qi, C.L. Chang, J. Xia, Speckleless holographic display by complex modulation based on double-phase method, *Opt. Express* 24 (2016) 30368–30378, <https://doi.org/10.1364/oe.24.030368>.
- [23] H. Pang, J.Z. Wang, A. Cao, M. Zhang, L.F. Shi, Q.L. Deng, Accurate hologram generation using layer-based method and iterative Fourier transform algorithm, 8–8, *IEEE Photonics J.* 9 (2017), <https://doi.org/10.1109/jphot.2016.2634783>.
- [24] H. Pang, J.Z. Wang, A.X. Cao, Q.L. Deng, High-accuracy method for holographic image projection with suppressed speckle noise, *Opt. Express* 24 (2016) 22766–22776, <https://doi.org/10.1364/oe.24.022766>.
- [25] P. Sun, S.Q. Chang, S.Q. Liu, X. Tao, C. Wang, Z.R. Zheng, Holographic near-eye display system based on double-convergence light Gerchberg-Saxton algorithm, *Opt. Express* 26 (2018) 10140–10151, <https://doi.org/10.1364/oe.26.010140>.
- [26] P.C. Zhou, Y. Bi, M.Y. Sun, H. Wang, F. Li, Y. Qi, Image quality enhancement and computation acceleration of 3D holographic display using a symmetrical 3D GS algorithm, *Appl. Opt.* 53 (2014) G209–G213, <https://doi.org/10.1364/ao.53.00g209>.
- [27] H. Pang, W.J. Liu, A.X. Cao, Q.L. Deng, Speckle-reduced holographic beam shaping with modified Gerchberg-Saxton algorithm, *Opt. Commun.* 433 (2019) 44–51, <https://doi.org/10.1016/j.optcom.2018.09.076>.
- [28] R.W. Gerchberg, W.O. Saxton, A practical algorithm for determination of phase from image and diffraction plane pictures, *Optik* 35 (1972) 237–246.
- [29] G. Sinclair, J. Leach, P. Jordan, G. Gibson, E. Yao, Z.J. Laczik, M.J. Padgett, J. Courtial, Interactive application in holographic optical tweezers of a multi-plane Gerchberg-Saxton algorithm for three-dimensional light shaping, *Opt. Express* 12 (2004) 1665–1670, <https://doi.org/10.1364/opex.12.001665>.
- [30] H.T. Chang, H.E. Hwang, C.L. Lee, Position multiplexing multiple-image encryption using cascaded phase-only masks in Fresnel transform domain, *Opt. Commun.* 284 (2011) 4146–4151, <https://doi.org/10.1016/j.optcom.2011.04.065>.